17,09

Self–assemble kinetic of Clusters of endohedral metallofullerenes in a polar solvent

© E.K. Alidzhanov[1], I.E. Kareev[2,¶], V.P. Bubnov[2], A.I. Kotov[2], S.N. Letuta[1], Yu.D. Lantukh[1], D.A. Razdobreev[1]

[1] Orenburg State University, Orenburg, Russia
[2] Federal Research Center of Problems of Chemical Physics and Medicinal Chemistry RAS, Chernogolovka, Russia

¶ E-mail: kareev@icp.ac.ru

Received June 14, 2023
Revised July 3, 2023
Accepted July 13, 2023

The evolution of the morphological properties of solutions of endohedral metallofullerene La@C_{82} in *N*, *N*-dimetilformamide in the presence of a coagulant was studied by dynamic and static light scattering methods. Based on the experimental results, the time evolution of the light scattering intensity, and the hydrodynamic radius of endohedral metallofullerene clusters, their association constants and aggregation rates are determined. Based on the analysis of the angular dependences of light scattering in solutions of endohedral metallofullerenes, the fractal dimension of La@C_{82} clusters in solutions of various concentrations at the initial and final stages of their aggregation was estimated.

Keywords: endohedral metallofullerenes, aggregation, dynamic and static light scattering, fractal clusters.

DOI: 10.61011/PSS.2023.09.57123.112

1. Introduction

Aggregation of fullerene nanoparticles in solutions and physical and chemical properties of such nanostructures draw close attention of researchers due to real prospects of application [1–4]. It has been found that, when the interaction energy between particles is comparable with the thermal field energy, diffusion-limited aggregation (DLA) model is implemented. If for cluster growth, a system activation stage is required resulting in irreversible coagulation, reactivity-limited aggregation (RLA) takes place [2]. Depending on the aggregation period time, the process may be treated either as kinetic or as quasi-equilibrium [2,5].

A fullerene solution is a high-dispersion system containing fullerene clusters whose hydrodynamic radii vary from units to hundreds nanometers [2,6,7]. Fullerene aggregation is characterized by formation of fractal type clusters with fractal number D_f within the range from 1.2 to 2.8 [6,8,9].

According to the available literature, qualitative characteristics of the fullerene aggregation have been evaluated so far using only kinetic approach, and the key quantitative parameters have been obtained by the nonequilibrium thermodynamics methods. However, the DLA model assumes that the aggregation may be treated within a short observation time as an quasi-equilibrium process for which equilibrium thermodynamics methods are applicable. Key parameters characterizing the equilibrium aggregation include free Gibbs energy G_F, appropriate variation of entalphy ΔH_F and entropy ΔS_F, equilibrium aggregation constant K_F of a colloid system.

Despite a well-developed reversible aggregation region of small molecules in a solution, no data is reported regarding the Gibbs energy variation ΔG_F or K_F for any type of fullerenes, except some theoretical studies [10–12].

Recently with nanotechnology advancement, identification of fundamental laws and physical and chemical features of synthesis of nanoscale structures with targeted properties is of special interest. Static and dynamic light scattering [13–15], methods of scanning tunneling and atomic-force microscopy [16,17] are used as the main high-sensitivity methods for nanostructure control.

The objective of the study was to investigate experimentally self-organization of La@C_{82} endohedral metallofullerene (EMF) molecules into fractal clusters in polar solvent solutions with changing ionic strength. It has been demonstrated that some key properties of the fullerene aggregation may be derived directly from experimental data.

2. Experiment procedure

Carbon black containing EMF with lanthanum was prepared by composite graphite electrode evaporation in an arc reactor developed and fabricated by us [18–20]. EMF was extracted from the carbon black by o-dichlorobenzene ($\geq$ 99% (GC), Sigma-Aldrich) in argon atmosphere at solvent boiling temperature. Isomerically pure La@$C_{82}(C_{2v})$ EMF was prepared by the multistage semi-preparative high performance liquid chromatography (HPLC) with sequential use of Cosmosil Buckyprep (10×250 mm) and Riges Buckyclutcher (10×250 mm) columns with two types of

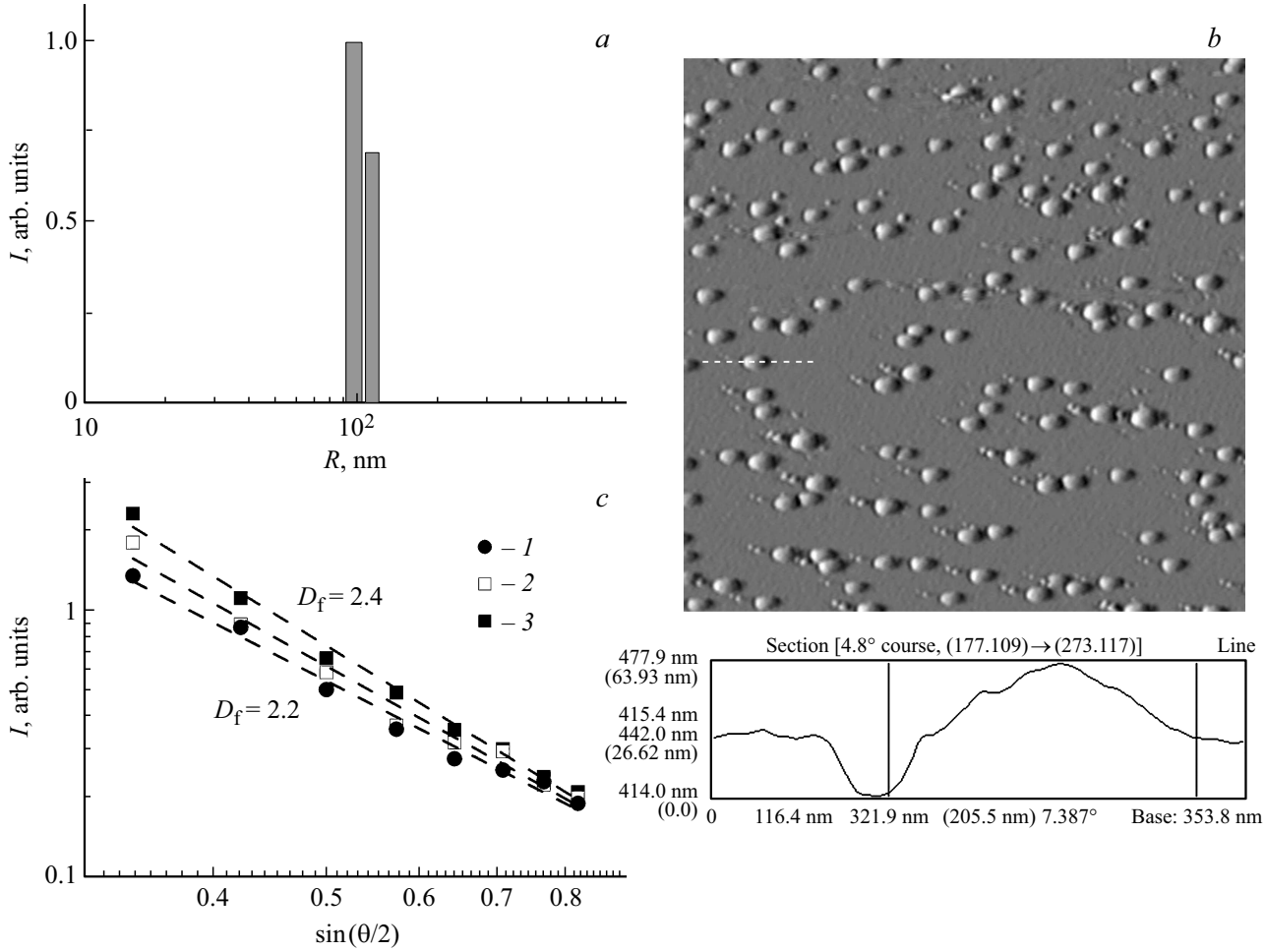

Figure 1. *a* — bar chart of EMF cluster distribution over hydrodynamic radii R nm in stock solution; *b* — AFM image of $6 \times 6\,\mu$m mica surface covered with EMF solution made after solvent removal, and EMF cluster peak profile distribution measured along the dashed line; *c* — angular dependences of the normalized light scattering intensity of the EMF stock solutions with various concentration: *1* — $C_0 = 1.5 \cdot 10^{-5}$ M; *2* — $C_0 = 3 \cdot 10^{-5}$ M; *3* — $C_0 = 5.5 \cdot 10^{-5}$ M.

sorbents. Toluene (ACS), 310 nm UV detector, was used as the mobile phase. La@C_{82} EMF (isomer C_{2v}) in toluene was characterized according to a procedure described in detail in [21,22].

La@C_{82} stock solution in N,N-dimethylformamide (DMFA, CP, EKOS-1) with concentration $3 \cdot 10^{-4}$ M was prepared. Further, the EMF solution concentration was varied by dilution. Additionally, EMF concentration in solutions was controlled by optical absorption spectra using the reported molar extinction coefficient of La@C_{82} [23].

The dynamic light scattering (DLS) method was used to study the EMF nanocluster distribution over the hydrodynamic radii in the solution. Measurements were carried out using Photocor Compact-Z analyzer with scattering angle 90°. $\lambda = 654$ nm semiconductor laser was used as an emission source.

The multi-angle (40–130°) static light scattering method was implemented on a in-house laboratory unit using helium-neon laser ($\lambda = 632$ nm) and PMT-68 (Photomultiplier Tube) complete with interference filter.

EMF nanocluster formation on the mica substrate was examined by the atomic-force microscopy (AFM) method. SMM-2000 microscope was used for contact-mode measurements. The samples were prepared by pouring EMF solutions onto the mica surface followed by solution removal.

3. Experimental results and discussion

Evolution of photophysical and morphological properties of La@C_{82} EMF solution in DMFA with addition of hydrochloric acid as a coagulating agent was studied. It is known from the coagulation theory that particle aggregation rate in a colloidal solution may be changed by varying coagulating agent concentration.

Solutions with three different concentrations were examined: № 1 — $C_0 = 1.5 \cdot 10^{-5}$ M; № 2 — $C_0 = 3 \cdot 10^{-5}$ M; № 3 — $C_0 = 5.5 \cdot 10^{-5}$ M. In all three solutions, whatever their concentration, identical monodisperse distribution of EMF clusters by hydrodynamic radii $R \approx 100$ nm was observed (Figure 1, *a* and *b*).

For fractal clusters, when $q^{-1} \leq R$ is satisfied for the scattering wave vector $q = 4\pi n/\lambda \sin(\theta/2)$ (herein λ is the light wavelength, θ is the scattering angle, n is the refraction index of the solution), there is an exponential dependence of scattering intensity on q [24]:

$$I(q) \propto q^{-D_f}. \quad (1)$$

Angular dependences of light scattering intensity of three EMF solution concentrations were measured. Measurements were corrected for scattering intensity by the solvent and by increasing solution volume to form a positive signal with deviation from $\theta = \pi/2$. The obtained dependences of light scattering intensity on $\sin(\theta/2)$ in logarithmic scale are shown in Figure 1, *c*.

Experimental data are reasonably approximated by linear dependences whose angular coefficient was used to estimate the fractal dimension of EMF clusters. It was found that the fractal dimension of EMF clusters increases with increasing solution concentration from $D_f = 2.2$ to $D_f = 2.4$. While the EMF cluster distribution by hydrodynamic radii remains unchanged.

It is shown in [25] that EMF clusters are resistant to ambient temperatures and UV exposure. Electrokinetic potential measurements in the EMF clusters in the DMFA solution show that negative zeta potential $\xi = -25 \text{—} -26$ mV is present and probably causes their stability. Addition of coagulating agent to solutions is followed by decrease of zeta potential to $\xi = -5$ mV, which probably initiates the EMF cluster aggregation process.

Hydrodynamic radii variation kinetics of EMF clusters during aggregation was studied by the DLS method. Light scattering intensity variation kinetics of the colloidal system was recorded at the same time.

Figure 2 shows normalized kinetic dependences of relative light scattering intensity variation in EMF solutions in DMFA after coagulating agent addition. This figure also shows hydrodynamic radii variation kinetics curves of EMF clusters during aggregation.

Figure 2, *a* shows the data for EMF solution № 1 measured after addition of 1/10 part of hydrochloric acid to the initial volume (2 mL). Time to achieve the stabilization condition (time to achieve the plateau for the light scattering intensity variation kinetics) was $t_{\text{stab}} = 3400$ s, initial hydrodynamic radius of clusters was $R_0 \approx 100$ nm, fractal dimension of clucters was $D_f = 2.2$. As shown in the data provided in Figures 2, *a*, hydrodynamic radii growth kinetics of EMF clusters is described by $R \propto t^{1/D_f}$ that agrees with the diffusion-limited aggregation (DLA) model [26].

Figure 2, *b* shows the data for EMF solution № 2 measured after addition of 1/20 part of hydrochloric acid to the initial volume (2 mL). In this case, the time to achieve the stabilization condition was $t_{\text{stab}} = 14\,000$ s, initial hydrodynamic radius of clusters was $R_0 \approx 100$ nm, fractal dependence of clusters was $D_f = 2.3$. hydrodynamic radius growth kinetics of EMF clusters in this case is linear and corresponds to an intermediate case between DLA and RLA models.

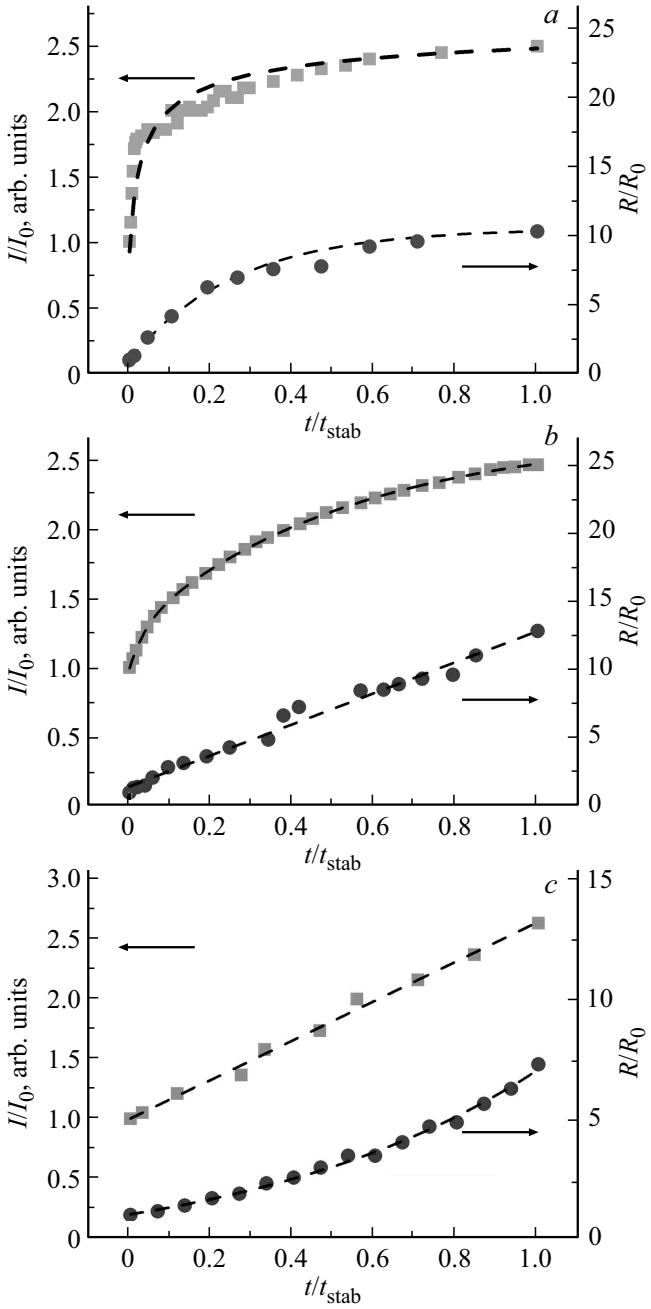

Figure 2. Lefthand axis — of DMFA light scattering variation kinetics of the EMF solution after addition of the coagulating agent to the solution. Righthand axis — hydrodynamic radius variation kinetics of EMF clusters. *a*) $C_0 = 1.5 \cdot 10^{-5}$ M, $R_0 = 100$ nm, added 200 μL hydrochloric acid, $t_{\text{stab}} = 3400$ s; *b*) $C_0 = 3 \cdot 10^{-5}$ M, $R_0 = 100$ nm, added 100 μL hydrochloric acid, $t_{\text{stab}} = 14\,000$ s; *c*) $C_0 = 5 \cdot 10^{-5}$ M, $R_0 = 100$ nm, added 50 μL hydrochloric acid, $t_{\text{stab}} = 14\,500$ s.

Figure 2, *a* shows the data for EMF solution № 3 measured after addition of 1/40 part of hydrochloric acid to the initial volume (2 mL). For this solution, the time to achieve the stabilization condition was $t_{\text{stab}} = 14\,500$ s, initial hydrodynamic radius of clusters was $R_0 \approx 100$ nm,

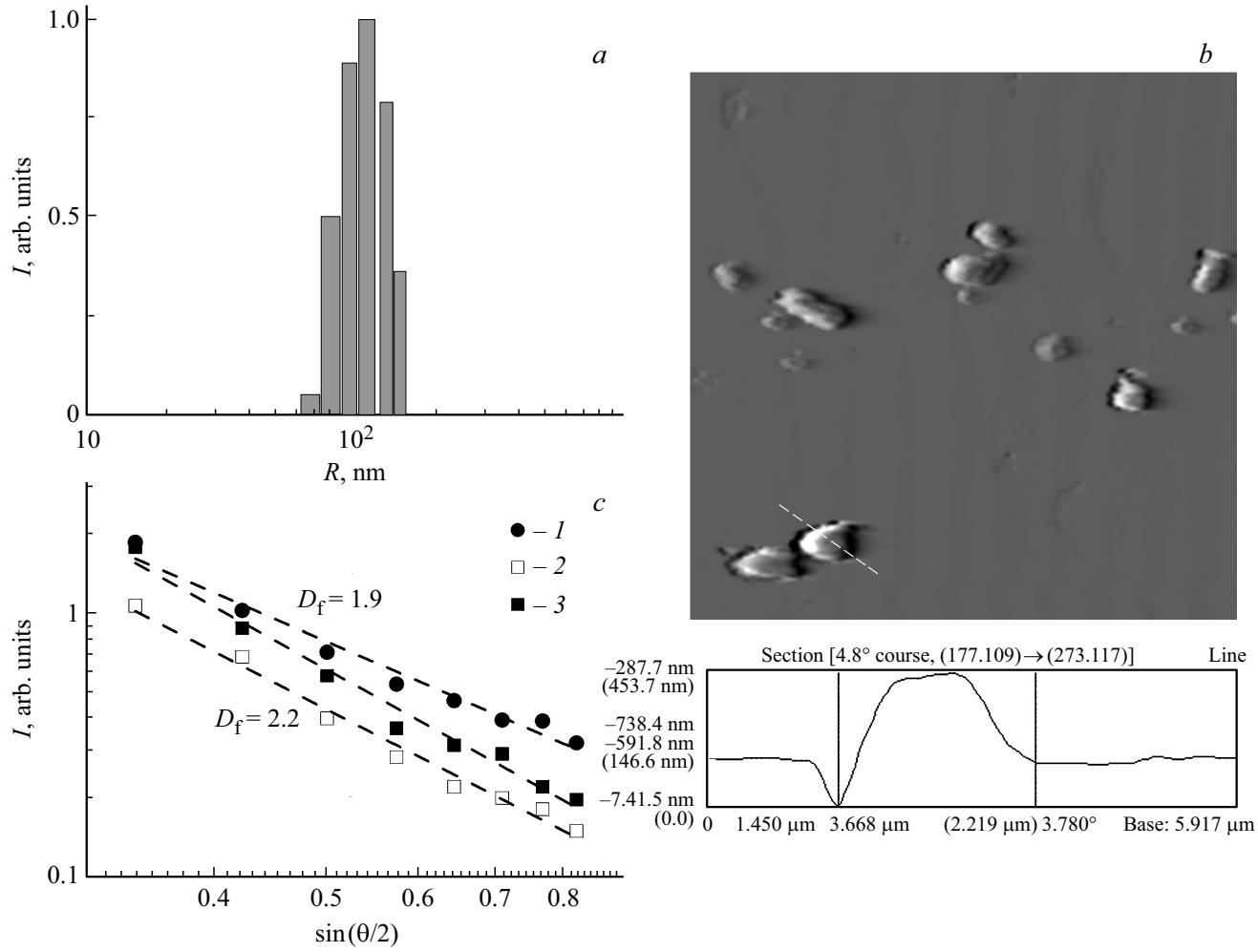

Figure 3. *a* — bar chart of EMF cluster distribution by hydrodynamic radii ($R \approx 1000$ nm) in the solution after achievement of the stabilization condition; *b* — AFM image of $16 \times 16\,\mu$m mica surface covered by the EMF solution made after solvent removal, and EMF cluster peak profile distribution measured along the dashed line; *c* — angular dependences of the normalized light scattering intensity of EMF solutions № 1, 2 and 3 measured at the final aggregation stage.

fractal dependence of clusters was $D_f = 2.4$. In this case, the hydrodynamic radius variation kinetics of EMF clusters is described by $R \propto R_0 e^{Ct}$ and agrees with the reactivity-limited aggregation (RLA) model [26].

Figure 3, *a* and *b* show the bar chart of EMF cluster distribution by hydrodynamic radii and AFM image. Measurements were carried out after stabilization of EMF solution aggregation. In all three test solutions, whatever their concentration, identical monodisperse distribution of EMF clusters by hydrodynamic radii was observed. Tenfold increase of EMF cluster sizes $R \approx 1000$ nm is observed.

While the cluster distribution by hydrodynamic radii remains close to a monodisperse type. Figure 3, *c* shows angular dependences of light scattering intensity measured for three solutions.

Experimental data are reasonably approximated by linear dependences whose angular coefficient was used to estimate the fractal dimension of EMF clusters. Fractal dimension of EMF clusters after achievement of the aggregation stabilization condition: for solution № 1 $D_f = 1.9$; for solution № 2 $D_f = 2.2$; for solution № 3 $D_f = 2.4$.

The data in Figure 2 show that the light scattering signal intensity of colloidal EMF solutions increases by a factor of 2.5–2.6 when the colloidal solution is achieving its stable state. The degree of light scattering signal increase does not depend on the solution concentration and amount of coagulating agent. Only the coagulation kinetics behavior changes.

Using the simultaneous measurements of time evolution of light scattering intensity $I(q, t)$ and hydrodynamic cluster radius $R_h(t)$, EMF cluster aggregation rate constants may be estimated at various process stages. In [27,28], colloidal solution aggregation rate constant calculation algorithm is offered on the basis of the analysis of $I(q, t)$ and $R_h(t)$ using the Rayleigh –Debye–Gans (RDG) scattering theory [29]. However, for large fractal clusters with sizes from 100 nm to 1000 nm, the use of the RDG theory is inappropriate. In our opinion, analysis of the obtained results using the

scaling approach and fractal dimension concept is more meaningful [24]. Within this approach, the number of elementary scatterers in the cluster is determined as

$$N = \left(\frac{R}{a}\right)^{D_f}, \tag{2}$$

here, R is the cluster radius, a is the elementary scatterer radius (EMF molecules), D_f is the fractal dimension of a cluster.

In a monomolecular state, intensity of light scattering by solution is proportional to the concentration of elementary scatterers in it $I(q) \propto N_0$. In case of formation of fractal clusters, elementary scatterers are grouped into compact systems of N monomers. If N of the scattering centers are within the distance q^{-1} from each other, then the scattered wave phase will be actually the same. However, secondary waves will be in the phase and added structurally. Then, the total scattering intensity will be proportional to $I(q) \propto N^2$. At $R > q^{-1}$, scattering intensity will increase in proportion to the number q^{-1} of regions included in the cluster. This is considered by introduction of a structural factor.

$$I(q) \propto N^2 (qR)^{-D_f}. \tag{3}$$

According to the foregoing, let's estimate the light scattering intensity variation of the colloidal solution after its full transition from monomolecular to cluster state.

In our case, the cluster radius satisfies $R_k > q^{-1}$. Assuming that all monomers N_0 in the solution change for the cluster form, we get the following expression:

$$I(qR) \propto \frac{N_0}{(R_k/a)^{D_f}} (R_k/a)^{2D_f} (qR_k)^{-D_f}$$

$$= N_0 (R_k/a)^{D_f} (qR_k)^{-D_f} = N_0 \frac{1}{(aq)^{D_f}}. \tag{4}$$

I. e. the light scattering signal increases by a factor of $(aq)^{-D_f}$ (by a factor of $\sim 10^3$ in our case) relative to the initial light scattering signal of the monomer solution. However, (if $R > q^{-1}$) the solution light scattering intensity does not depend on the radius of the formed clusters R_k. Light scattering intensity of the colloidal solution depends only on the amount of monomers switched to the cluster form.

For the EMF solutions of interest, the light scattering intensity at the initial stage is composed of the signals from the cluster and monomer components. ($I_0 = I_K + I_M$).

According to the offered model

$$I_K \propto (N_0 - N_1)(aq)^{-D_f}, \quad I_M \propto N_1$$

(herein, N_0 is the total monomer concentration, N_1 is the proportion of nonclusterized monomers).

At the final aggregation kinetics stage, all monomers change to the aggregate state.

$$I_{max} = I_K \propto N_0 (aq)^{-D_f}. \tag{5}$$

As shown in Figure 2, the light scattering signal intensity increases by a factor of 2.5–2.6. Therefore, the following proportion may be derived:

$$\frac{I_0}{I_{max}} \propto \frac{(N_0 - N_1)(aq)^{-D_f} + N_1}{N_0 (aq)^{-D_f}} \approx \frac{(N_0 - N_1)}{N_0} \approx 0.4 \tag{6}$$

(it is assumed here that $I(N_1)$ has the third order of smallness).

Hence, $N_1 \approx 0.6 N_0$, that meets the association factor $K_F \approx (0.1–0.4) \cdot 10^5\ M^{-1}$.

When measuring the cluster growth kinetics by the DLS method, small-size cluster formation was not observed. Based on the shown findings, it can be suggested that the light scattering signal variation kinetics is defined by the degree of monomer association to the cluster phase. At the initial stage, before coagulating agent addition, $I_0/I_{max} \approx 0.4$ part of monomers (0.6 part was not involved) was involved in cluster formation. At the final coagulation stage, all particles in the solution were in the cluster state. The amount of monomers that change to the cluster form may be defined as $\frac{I(t)}{I_{max}} N_0$ (here N_0, $cm^{-3} = C_0 N_A/1000$ is the amount of monomers per unit volume of the stock solution). Cluster concentration N_k in the solution may be determined by the ratio of the total amount of monomers in the cluster form and the amount of monomers in an individual cluster

$$N_k(t) = \frac{I(t)}{I_{max}} N_0 \left(\frac{R(t)}{a}\right)^{-D_f}. \tag{7}$$

At the initial coagulation stage, the coagulation process is driven both by attachment of free monomers to clusters and by cluster-cluster aggregation.

At the final coagulation stage, almost all monomers change to the cluster fraction and only cluster-cluster aggregation takes place. EMF cluster concentration variation N_k form initial value N_{k0} or cluster-cluster aggregation may be described by the Smoluchowski equation written as follows:

$$\frac{dN_k}{dt} = \frac{k_{nn}}{2} N_k^2, \tag{8}$$

where k_{nn} is the cluster-cluster aggregation rate constant.

When monomers are attached to large clusters, the probability of the inverse process is extremely low [28]. Therefore, unlike the chemical process kinetics, the aggregation rate constant in the Smoluchowski equation is multiplied by 1/2. Solution of this kinetic equation may be written as

$$1/N_k = 1/N_{k0} + \frac{k_{nn}}{2} t. \tag{9}$$

Figure 4 shows the calculation of time evolution of inverse concentration of EMF clusters according to the experimental data shown in Figure 2. Initial and final segments of the plotted kinetic curve may be approximated by linear dependences whose slope defined the cluster–cluster aggregation rate constant in the EMF solutions.

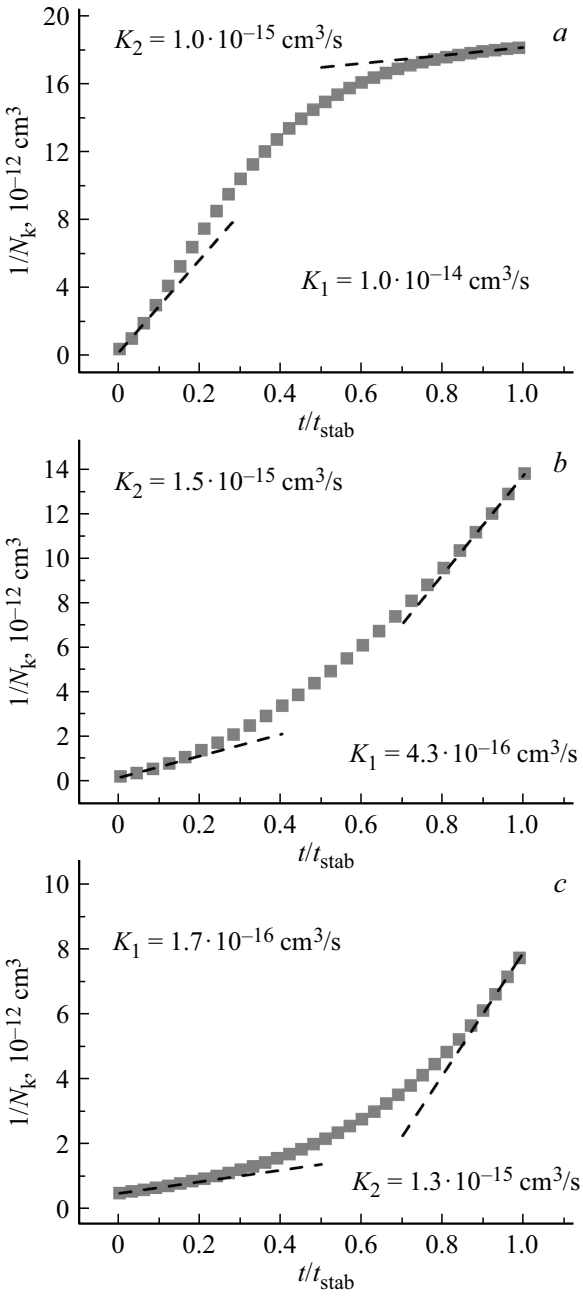

Figure 4. Calculation of concentration variation kinetics for the EMF clusters in the DMFA solution during aggregation. K_1 and K_2 correspond to the slope of initial and final segments of the plotted kinetic curves. *a*) $C_0 = 1.5 \cdot 10^{-5}$ M, added *a*) 200 μL hydrochloric acid, $C_0 = 1.5 \cdot 10^{-5} t_{stab} = 3400$ s; *b*) $C_0 = 3 \cdot 10^{-5}$ M, added *b*) 100 μL hydrochloric acid, $C_0 = 3 \cdot 10^{-5} t_{stab} = 14\,000$ s; *c*) $C_0 = 5 \cdot 10^{-5}$ M, added *c*) 50 μL hydrochloric acid, $C_0 = 5 \cdot 10^{-5} t_{stab} = 14\,500$ s.

For rapid coagulation (DLA), cluster–cluster aggregation rate constant at the initial coagulation stage is equal to $k_{nn}/2 = 10^{-14}$ cm^3/s, at the final stage is equal to $k_{nn}/2 = 10^{-15}$ cm^3/s (Figure 4, *a*).

For slow coagulation (RLA), cluster–cluster aggregation rate constant at the initial coagulation stage is equal to $k_{nn}/2 = 1.7 \cdot 10^{-16}$ cm^3/s, at the final stage is equal to $k_{nn}/2 = 1.3 \cdot 10^{-15}$ cm^3/s (Figure 4, *a*).

For the intermediate case (Figure 4, *b*), cluster–cluster aggregation rate constant at the initial coagulation stage is equal to $k_{nn}/2 = 4.3 \cdot 10^{-16}$ cm^3/s, at the final stage is equal to $k_{nn}/2 = 1.5 \cdot 10^{-15}$ cm^3/s .

Aggregation of free monomers with EMF clusters may be described by the Smoluchowski equation as follows:

$$\frac{dN_k}{dt} = \frac{k_{1n}}{2} N_1 N_k, \tag{10}$$

here, N_1 and N_k are initial concentrations of monomers and clusters, k_{1n} is the monomer–cluster aggregation rate constant.

Using the relation between the kinetic dependence of the light scattering intensity and the cluster concentration in the EMF solution of interest, the following may be written

$$\frac{dN_k}{dt} = \frac{d\left(\frac{I(t)}{I_{\max}}\right) N_0 \left(\frac{R_k}{a}\right)^{-D_f}}{dt} = \frac{k_{1n}}{2} N_k N_1. \tag{11}$$

If the cluster and free monomer concentration in the last expression is expressed in terms of the initial monomer concentration, we get the following relation:

$$\frac{dN_k}{dt} = \frac{d\left(\frac{I(t)}{I_{\max}}\right) N_0 \left(\frac{R_k}{a}\right)^{-D_f}}{dt} = \frac{k_{1n}}{2} N_k N_1$$
$$= \frac{k_{1n}}{2} N_0 \frac{I(t)}{I_{\max}} \left(\frac{R_k}{a}\right)^{-D_f} N_0 \left(1 - \frac{I(t)}{I_{\max}}\right). \tag{12}$$

After reduction of similar terms in the left and right parts of the relation above, we get the expression for coagulation rate constant evaluation

$$\frac{k_{1n}}{2} = \frac{d\left(\frac{I(t)}{I_{\max}}\right)}{dt} N_0^{-1} \left(\frac{I(t)}{I_{\max}} - \left(\frac{I(t)}{I_{\max}}\right)^2\right)^{-1}. \tag{13}$$

Derivative $\frac{d\left(\frac{I(t)}{I_{\max}}\right)}{dt}$ is determined from the relevant curve of kinetic dependence of light scattering intensity (Figure 2).

The calculation shows that for rapid coagulation (DLA) case, the monomer — cluster aggregation rate constant is equal to $k_{n1}/2 = 8.4^{-18}$ cm^3/s. For slow coagulation (RLA),the aggregation rate constant is equal to $k_{n1}/2 = 2.7 \cdot 10^{-20}$ cm^3/s. For the intermediate case, the aggregation rate constant is equal to $k_{n1}/2 = 1.1 \cdot 10^{-19}$ cm^3/s.

From the derived k_{n1}, it follows that the monomer–cluster aggregation makes a low contribution to the cluster dimension variation, but contributes decisively to the light scattering signal variation.

4. Conclusion

Time evolution of the light scattering intensity and hydrodynamic radii of the EMF clusters in DMFA with

coagulating agent addition to the stock solution has been studied. It is shown that conditions for implementation of various coagulation kinetics models (DLA, RLA) may be formed by varying the amount of coagulating agent and EMF concentration in the solution. Dependences of light scattering intensity by system N_0 of elementary scatterers transferred to the fractal cluster form on the effective cluster radius and fractal dimension. Based on the formed simulated representations and obtained kinetic dependences, factor of association of EMF molecules to cluster form was derived. EMF cluster concentration variation kinetics during aggregation was studied for three various coagulation models (DLA, RLA, intermediate case). EMF cluster aggregation rate constants were defined at the initial and final process stages. Based on the analysis of angular dependences of light scattering by EMF solutions, fractal dimension of $La@C_{82}$ clusters for solutions with various concentration was evaluated at the initial and final aggregation stages.

Funding

The study was performed under the State Assignment of the Ministry of Science and Higher Education of the Russian Federation (State registration No. AAAA-A19-119092390079-8 and FSGU-2023-0003, State registration No. 123012500132-4).

Conflict of interest

The authors declare that they have no conflict of interest.

References

[1] D.Y. Lyon, L.K. Adams, J.C. Falkner, P.J.J. Alvarez. Environ. Sci. Technol. **40**, *14*, 4360 (2006).
[2] N.O. Mchedlov-Petrossyan. Chem. Rev. **113**, *7*, 5149 (2013).
[3] A. Astefanei, O. Núñez, M.T. Galceran. Anal. Chim. Acta **882**, 1 (2015).
[4] N. Aich, L.K. Boateng, I.V. Sabaraya, D. Das, J.R. Flora, N.B. Saleh. Environ. Sci. Technol. **50**, *7*, 3562 (2016).
[5] S. Nath, H. Pal, A.V. Sapre, J.P. Mittal. J. Photosci. **10**, *1*, 105 (2003).
[6] M.V. Suyasova, Y.V. Kul'Velis, V.T. Lebedev, V.P. Sedov. Russ. J. Appl. Chem. **88**, *11*, 1839 (2015).
[7] U. Ritter, Y.I. Prylutskyy, M.P. Evstigneev, N.A. Davidenko, V.V. Cherepanov, A.I. Senenko, A.G. Naumovets. Fuller. Nanotub. Carbon Nanostruct. **23**, *6*, 530 (2015).
[8] Z. Meng, S.M. Hashmi, M. Elimelech. J. Colloid Interface Sci. **392**, 27 (2013).
[9] J. Gigault, B. Grassl. J. Colloid Interface Sci. **502**, 193 (2017).
[10] X. Zhao, A. Striolo, P.T. Cummings. Biophys. J. **89**, *6*, 3856 (2005).
[11] D.P. Voronin, A.S. Buchelnikov, V.V. Kostjukov, S.V. Khrapatiy, D. Wyrzykowski, J. Piosik, M.P. Evstigneev. J. Chem. Phys. **140**, *10*, 104909 (2014).
[12] Y.I. Prylutskyy, A.S. Buchelnikov, D.P. Voronin, V.V. Kostjukov, U. Ritter, J.A. Parkinson, M.P. Evstigneev. Phys. Chem. Chem. Phys. **15**, *23*, 9351 (2013).
[13] Yu.I. Prylutskyy, V.V. Cherepanov, M.P. Evstigneev, O.A. Kyzyma, V.I. Petrenko, V.I. Styopkin, L.A. Bulavin, N.A. Davidenko, D. Wyrzykowski, A. Woziwodzka, J. Piosik, R. Kaźmierkiewicz, U. Ritter. Phys. Chem. Chem. Phys. **17**, *39*, 26084 (2015).
[14] Z. Luo, D. Marson, Q.K. Ong, A. Loiudice, J. Kohlbrecher, A. Radulescu, A. Krause Heuer, T. Darwish, S. Balog, R. Buonsanti, D.I. Svergun, P. Posocco, F. Stellacci. Nature Commun. **9**, *1*, 1343 (2018).
[15] M.J. Hollamby, C.F. Smith, M.M. Britton, A.E. Danks, Z. Schnepp, I. Grillo, B.R. Pauw, A. Kishimura, T. Nakanish. Phys. Chem. Chem. Phys. **20**, *5*, 3373 (2018).
[16] D.A. Olyanich, V.V. Mararov, T.V. Utas, A.V. Zotov, A.A. Saranin. Surf. Sci. **653**, 138 (2016).
[17] V.D. Pham, V. Repain, C. Chacon, A. Bellec, Y. Girard, S. Rousset, S. Campidelli, J.S. Lauret, C. Voisin, M. Terrones, M.C. dos Santos, J. Lagoute. J. Phys. Chem. C **121**, *43*, 24264 (2017).
[18] I.E. Kareev, V.P. Bubnov, D.N. Fedutin. Tech. Phys. **54**, *11*, 1695 (2009).
[19] V.P. Bubnov, E.E. Laukhina, I.E. Kareev, V.K. Koltover, T.G. Prokhorova, E.B. Yagubskii, Y.P. Kozmin. Chem. Mater. **14**, *3*, 1004 (2002).
[20] I.E. Kareev, V.M. Nekrasov, V.P. Bubnov. Tech. Phys. **60**, *1*, 102 (2015).
[21] I.E. Kareev, V.P. Bubnov, E.B. Yagubskii. Russ. Chem. Bull. **56**, *11*, 2140 (2007).
[22] I.E. Kareev, V.M. Nekrasov, A.E. Dutlov, V.M. Martynenko, V.P. Bubnov, E. Laukhina, J. Veciana, C. Rovira. Russ. J. Phys. Chem. **91**, *3*, 536 (2017).
[23] K. Akiyama, K. Sueki, T. Kodama, K. Kikuchi, I. Ikemoto, M. Katada, H. Nakahara. J. Phys. Chem. A **104**, *31*, 7224 (2000).
[24] C.M. Sorensen. Aerosol Sci. Technol. **35**, *2*, 648 (2001).
[25] [I.E. Kareev, V.P. Bubnov, E.K. Alidzhanov, S.N. Pashkevich, Yu.D. Lantukh, S.N. Letuta, D.A. Razdobreev. Phys. Sold State **58**, *9*, 1924 (2016).
[26] Q. Ying, J. Marecek, B. Chu. J. Chem. Phys. **101**, *4*, 2665 (1994).
[27] S. Xu, Z. Sun. Soft Matter **7**, *24*, 11298 (2011).
[28] H. Holthoff, A. Schmitt, A. Fernández-Barbero, M. Borkovec, M.Á. Cabrerízo-Vılchez, P. Schurtenberger, R. Hidalgo-Álvarez. J. Colloid Interface Sci. **192**, *2*, 463 (1997).
[29] H. Holthoff, M. Borkovec, P. Schurtenberger. Phys. Rev. E **56**, *6*, 6945 (1997).

Translated by E.Ilyinskaya